

1 An evaluation of IASI-NH₃ with ground-based FTIR 2 measurements

3 Enrico Dammers¹, Mathias Palm², Martin Van Damme^{1,3}, Corinne Vigouroux⁴, Dan Smale⁵, Stephanie Conway⁶,
4 Geoffrey C. Toon⁷, Nicholas Jones⁸, Eric Nussbaumer⁹, Thorsten Warneke², Christof Petri², Lieven Clarisse³,
5 Cathy Clerbaux³, Christian Hermans⁴, Erik Lutsch⁶, Kim Strong⁶, James W. Hannigan⁹, Hideaki Nakajima¹⁰,
6 Isamu Morino¹¹, Beatriz Herrera¹², Wolfgang Stremme¹², Michel Grutter¹², Martijn Schaap¹³, Roy J. Wichink
7 Kruit¹⁴, Justus Notholt², Pierre.-F. Coheur³ and Jan Willem Erisman^{1,15}

8 1. Cluster Earth and Climate, Department of Earth Sciences, Vrije Universiteit Amsterdam, Amsterdam, the
9 Netherlands

10 2. Institut für Umweltphysik, University of Bremen, Bremen, Germany

11 3. Spectroscopie de l'Atmosphère, Service de Chimie Quantique et Photophysique, Université Libre de Bruxelles
12 (ULB), Brussels, Belgium

13 4. Royal Belgian Institute for Space Aeronomy (BIRA-IASB), Brussels, Belgium

14 5. National Institute of Water and Atmosphere, Lauder, New Zealand

15 6. University of Toronto, Toronto, Ontario, Canada

16 7. Jet Propulsion Laboratory, California Institute of Technology, Pasadena

17 8. University of Wollongong, Wollongong, Australia

18 9. NCAR, Boulder, Colorado, United States

19 10. Atmospheric Environment Division, National Institute for Environmental Studies (NIES), Japan

20 11. National Institute for Environmental Studies, 16-2 Onogawa, Tsukuba, Ibaraki, 305-8506, Japan

21 12. Centro de Ciencias de la Atmosfera, Universidad Nacional Autonoma de Mexico, Mexico City, Mexico

22 13. TNO Built Environment and Geosciences, Department of Air Quality and Climate, Utrecht, the Netherlands

23 14. National Institute for Public Health and the Environment (RIVM), Bilthoven, the Netherlands

24 15. Louis Bolk Institute, Driebergen, the Netherlands

25

26 *Correspondence to:* E. Dammers (e.dammers@vu.nl)

27 **Abstract.** Global distributions of atmospheric ammonia (NH₃) measured with satellite instruments such as the
28 Infrared Atmospheric Sounding Interferometer (IASI) contain valuable information on NH₃ concentrations and
29 variability in regions not yet covered by ground based instruments. Due to their large spatial coverage and (bi-)
30 daily overpasses, the satellite observations have the potential to increase our knowledge of the distribution of
31 NH₃ emissions, and associated seasonal cycles. However the observations remain poorly validated, with only a
32 handful of available studies often using only surface measurements without any vertical information. In this
33 study, we present the first validation of the IASI-NH₃ product using ground-based Fourier Transform InfraRed
34 (FTIR) observations. Using a recently developed consistent retrieval strategy, NH₃ concentration profiles have
35 been retrieved using observations from nine Network for the Detection of Atmospheric Composition Change
36 (NDACC) stations around the world between 2008- 2015. We demonstrate the importance of strict spatio-
37 temporal collocation criteria for the comparison. Large differences in the regression results are observed for
38 changing intervals of spatial criteria, mostly due to terrain characteristics and the short lifetime of NH₃ in the
39 atmosphere. The seasonal variations of both datasets are consistent for most sites. Correlations are found to be
40 high at sites in areas with considerable NH₃ levels, whereas correlations are lower at sites with low atmospheric
41 NH₃ levels close to the detection limit of the IASI instrument. A combination of the observations from all sites
42 ($N_{\text{obs}} = 547$) give a MRD of $-32.4 \pm (56.3) \%$, a correlation r of 0.8 with a slope of 0.73. These results give an
43 improved estimate of the IASI-NH₃ product performance compared to the previous upper bound estimates (-
44 50% - +100%).

45 1. Introduction

46 Humankind has increased the global emissions of reactive nitrogen to an unprecedented level (Holland et al.,
47 1999; Rockström et al., 2009). The current global emissions of reactive nitrogen are estimated to be a factor four
48 larger than pre-industrial levels (Fowler et al., 2013). Consequently atmospheric deposition of reactive nitrogen
49 to ecosystems has substantially increased as well (Rodhe et al., 2002; Dentener et al., 2006). Ammonia (NH₃)
50 emissions play a major role in this deposition with a total emission of 49.3Tg in 2008 (Emission Database for
51 Global Atmospheric Research (EDGAR), 2011). Although NH₃ emissions are predominantly from agriculture in
52 the Northern Hemisphere, wildfires also play a role, with biomass burning contributing up to 8% of the global
53 emission budget (Sutton et al., 2013). NH₃ has been shown to be a major factor in the acidification and
54 eutrophication of soil and water bodies, which threatens biodiversity in vulnerable ecosystems (Bobbink et al.,
55 2010; Erisman et al., 2008, 2011). Through reactions with sulphuric and nitric acid, NH₃ also contributes to the
56 formation of particulate matter which is associated with adverse health effects (Pope et al., 2009). Particulate
57 ammonium salts contribute largely to aerosol loads over continental regions (Schaap et al., 2004). Through its
58 role in aerosol formation, NH₃ also has an impact on global climate change as hygroscopic ammonium salts are
59 of importance for the aerosol climate effect and thus the global radiance budget (Adams et al., 2001).
60 Furthermore increased NH₃ concentrations in the soil also enhance the emission of nitrous oxide (N₂O) which is
61 an important greenhouse gas and an ozone-depleting substance (Ravishankara et al., 2009). Finally nitrogen
62 availability is a key factor for the fixation of carbon dioxide (CO₂) and thus it is an important factor in climate
63 change.
64

65 Despite the fact that NH₃ at its current levels is a major threat to the environment and human health, relatively
66 little is known about its total budget and global distribution (Sutton et al., 2013; Erisman et al., 2007). Surface
67 observations are sparse and mainly available for north-western Europe, the United States and China (Van
68 Damme et al., 2015a). At the available sites, in situ measurements are mostly performed with relatively poor
69 temporal resolution due to the high costs of performing reliable NH₃ measurements with high temporal
70 resolution. These measurements of NH₃ are also hampered by sampling artefacts caused by the reactivity of NH₃
71 and the evaporation of ammonium nitrate (Slanina et al., 2001; von Bobruzki et al., 2010; Puchalski et al.,
72 2011). As the lifetime of atmospheric NH₃ is rather short, on the order of hours to a few days, due to efficient
73 deposition and fast conversion to particulate matter, the existing surface measurements are not sufficient to
74 estimate global emissions without inducing large errors. The lack of vertical profile information further hampers
75 the quantification of the budget, with only a few reported airborne measurements (Nowak et al., 2007, 2010,
76 Leen et al., 2013, Whitburn et al., 2015).

77 Advanced IR-sounders such as the Infrared Atmospheric Sounding Interferometer (IASI), the Tropospheric
78 Emission Spectrometer (TES), and the Cross-track Infrared Sounder (CrIS) enable retrievals of atmospheric
79 NH₃ (Beer et al., 2008; Coheur et al., 2009; Clarisse et al., 2009; Shephard et al., 2011, 2015a). The availability
80 of satellite retrievals provide a means to consistently monitor global NH₃ distributions. Global distributions
81 derived from IASI and TES observations have shown high NH₃ levels in regions not covered by ground-based
82 data. In this way, more insight was gained into known and unknown NH₃ sources worldwide including biomass
83 burning, industry and agricultural areas. Hence, satellite observations have the potential to improve our

84 knowledge of the distribution of global emissions and their seasonal variation due to their large spatial coverage
85 and (bi-) daily observations (Zhu et al., 2013; Van Damme et al., 2014b, 2015b; Whitburn et al., 2015; Luo et
86 al., 2015). However, the satellite observations remain poorly validated with only a few dedicated campaigns
87 performed with limited spatial, vertical or temporal coverage (Van Damme et al., 2015a; Shephard et al., 2015b,
88 Sun et al., 2015).

89 Only a few studies have explored the quality of the IASI-NH₃ product. A first evaluation of the IASI
90 observations was made over Europe using the LOTOS-EUROS model and has shown the respective consistency
91 of the measurements and simulations (Van Damme et al., 2014b). A first comparison using ground-based and
92 airborne measurements to validate the IASI-NH₃ data set were made in Van Damme et al. (2015a). They
93 confirmed consistency between the IASI-NH₃ data set and the available ground-based observations and showed
94 promising results for validation by using independent airborne data from the CalNex campaign. Nevertheless,
95 that study was limited by the availability of independent measurements and suffered from representativeness
96 issues for the satellite observations when comparing to surface concentration measurements. One of the key
97 conclusions was the need for vertical profiles (e.g. ground-based remote sensing products or upper-air in situ
98 measurements to compare similar quantities). Recently, Dammers et al. (2015) developed a retrieval
99 methodology for Fourier Transform Infrared Spectroscopy (FTIR) instruments to obtain remotely sensed
100 measurements of NH₃ and demonstrated the retrieval characteristics for four sites located in agricultural and
101 remote areas. Here we explore the use of NH₃ total columns obtained with ground based FTIR at nine stations
102 with a range of NH₃ pollution levels to validate the IASI-NH₃ satellite product by Van Damme (2014a).

103 First, we concisely describe the ground based FTIR retrieval and IASI-NH₃ product datasets in Sections 2.1 and
104 2.2. Next we describe the methodology of the comparison in Section 2.3 followed by the presentation of the
105 results in Section 3, which are then summarized and discussed in Section 4.

106

107 **2. Description of the satellite and FTIR data sets and validation methodology**

108 **2.1 IASI-NH₃ product**

109 The first global NH₃ distribution was obtained by a conventional retrieval method applied to IASI spectra
110 (Clarisse et al., 2009), followed by an in depth case study, using a more sophisticated algorithm, of the
111 sounder's capabilities depending on the thermal contrast (defined in Van Damme et al. (2014a) as the
112 temperature differences between the Earth surface and the atmosphere at 1.5 km altitude, Clarisse et al., 2010).
113 In this study we use the NH₃ product developed by Van Damme et al. (2014a). Their product is based on the
114 calculation of a dimensionless spectral index (Hyperspectral Range Index: HRI), which is a quantity
115 representative of the amount of NH₃ in the total atmospheric column. This HRI is then converted into NH₃ total
116 columns using look-up-tables based on numerous forward simulations for various atmospheric conditions.
117 These look-up-tables relate the HRI and the thermal contrast to a total column of NH₃ (Van Damme et al.,
118 2014a). The product includes an error characterization of the retrieved column based on errors in the thermal
119 contrast and HRI. Important advantages of this method over the method by Clarisse (2009) is the relatively
120 small computational cost, the improved detection limit and the ability to identify smaller emission sources and
121 transport patterns above the sea. One of the limitations of this method is the use of only two NH₃ vertical
122 profiles: a "source profile" for land cases and a "transported profile" for sea cases (Illustrated in Van Damme et
123 al., 2014a, fig. 3). Another limitation of the product is that it does not allow the calculation of an averaging
124 kernel to account for the vertical sensitivity of the instrument sounding to different layers in the atmosphere. In
125 this paper we will use NH₃ total columns retrieved from the IASI-A instrument (aboard of the MetOp-A
126 platform) morning overpass (AM) observations (i.e. 09:30 local time at the equator during overpass) which have
127 a circular footprint of 12 km diameter at nadir and an ellipsoid shaped footprint of up to 20 km x 39 km at the
128 outermost angles. We will use observations from January 1st 2008 to December 31st 2014. Figure 1 shows the
129 mean IASI-NH₃ total column distribution (all observations gridded to a 0.1° x 0.1° grid) using observations
130 above land for the years 2008-2014. The mean columns are obtained through a weighting with the relative error
131 (see Van Damme et al., 2014). The bottom left inset shows the corresponding relative error.

132

133

134 2.2 FTIR- NH₃ retrieval

135

136 The FTIR-NH₃ retrieval methodology used here is described in detail in Dammers et al. (2015) and a summary
137 is given here. The retrieval is based on the use of two spectral micro-windows, which contain strong individual
138 NH₃ absorption lines. The two spectral windows [930.32-931.32 cm⁻¹, MW1] and [962.70-970.00 cm⁻¹, MW2]
139 or the wider version for regions with very low concentrations [929.40-931.40 cm⁻¹, MW1 Wide] and [962.10-
140 970.00 cm⁻¹, MW2 Wide] are fitted using SFIT4 (Pougatchev et al., 1995; Hase et al., 2004, 2006) or a similar
141 retrieval algorithm (Hase et al, 1999) based on the optimal estimation method (Rodgers et al., 2000) to retrieve
142 the volume mixing ratios (in ppbv) and total columns of NH₃ (in molecules cm⁻²). Major interfering species in
143 these windows include H₂O, CO₂ and O₃. Minor interfering species are N₂O, HNO₃, CFC-12 and SF₆. For the
144 line spectroscopy, the HITRAN 2012 (Rothman et al., 2013) database is used with a few adjustments for CO₂
145 (ATMOS, Brown et al., 1996), and sets of pseudo-lines generated by NASA-JPL (G.C. Toon) are used for the
146 broad absorptions by heavy molecules (i.e. CFC-12, SF₆). The *a-priori* profiles of NH₃ are based on balloon
147 measurements (Toon et al., 1999) and scaled to fit common surface concentrations at each of the sites. An
148 exception is made for the a-priori profile at Reunion Island where a modelled profile from the MOZART model
149 is used (Louisa Emmons, personal communication, 2014). There, the profile peaks at a height of 4-5 km, as NH₃
150 are expected to be due to transport of biomass burning emissions on the island and Madagascar. For all stations,
151 the *a-priori* profiles for interfering species are taken from the Whole Atmosphere Community Climate Model
152 (WACCM, Chang et al., 2008). Errors in the retrieval are typically ~30% (Dammers et al., 2015), which are
153 mostly due to uncertainties in the spectroscopy in the line intensities of NH₃ and the temperature and pressure
154 broadening coefficients (HITRAN 2012).

155

156 An effort has been made to gather observations from most of the station part of the Network for the Detection of
157 Atmospheric Composition Change (NDACC) which have obtained relevant solar spectra between 1st of Jan
158 2008 and 31st of Dec 2014. We excluded stations which have only retrieved or are believed to have, NH₃ total
159 columns smaller than 5x10¹⁵ (molecules cm⁻²) during the study interval (i.e. Arctic and Antarctic and other
160 stations with concentrations below the expected limits of the IASI-NH₃ product, at best ~5x10¹⁵ for observations
161 with high thermal contrast). Figure 1 shows the positions of the FTIR stations used in this study. The retrieved
162 NH₃ total columns (molecules cm⁻²) for each of the stations are shown in Figure 2. The number of available
163 observations per station varies as does the range in total columns with high values of ~100x10¹⁵ (molecules cm⁻²)
164 observed at Bremen and low values of about 1x10¹⁵ (molecules cm⁻²) at St Denis Reunion. The following
165 provides a short description of each of the sites used in this study and retrieved NH₃ columns (molecules cm⁻²).
166 Additionally, a short summary can be found in Table 1:

167 The **Bremen** site operated on the university campus by the University of Bremen in the northern part of the city
168 (Velazco et al., 2007). Bremen is located in the northwest of Germany, which is characterized by intensive
169 agriculture. It is most suitable for comparisons with IASI given the very high observed concentrations (Fig. 2,
170 blue) and flat geography surrounding the station. NH₃ sources near the measurement station include manure
171 application to fields, livestock housing and exhaust emissions of local traffic. The retrieved NH₃ total columns
172 peak in spring due to manure application and show an increase in summer due to increased volatilization of NH₃
173 from livestock housing and fields when temperatures increase during summer.

174 The **Toronto** site (Wiacek et al., 2007) is located on the campus of the University of Toronto, Canada. The city
175 is next to Lake Ontario with few sources to the south. NH₃ sources are mainly due to agriculture as well as local
176 traffic in the city. Occasionally, NH₃ in smoke plumes from major boreal fires to the north and west of the city
177 can be observed (Lutsch et al., 2016). The retrieved columns (Fig. 2, green) show increased values during
178 summers as well as peaks in spring.

179 The **Boulder** observation site is located at the NCAR Foothills Lab in Boulder, Colorado, United States of
180 America, about 60 km northwest of the large metropolitan Denver area. It is located at 1.6 km a.s.l. on the
181 generally dry Colorado Plateau. Directly to the west are the foothills of the Rocky Mountain range and to the
182 east are rural grasslands, farming and ranching facilities. Among them are large cattle feed lots to the northeast
183 near Greeley approximately 90 km distant. The area is subject to occasional seasonal local forest fires and also
184 occasionally sees plumes from fires as distant as Washington or California. The retrieved columns (Fig. 2, grey)
185 show the largest increase during summers.

186 The **Tsukuba** site (Ohyama et al., 2009) is located at the National Institute for Environmental Studies (NIES),
187 in Japan. The region is a mixture of residential and rural zones with mountains to the north. NH₃ sources near
188 the measurement site include manure and fertilizer applications and exhaust emissions of local traffic in the
189 surrounding city with a large part originating from the from the Tokyo metropolitan area. The retrieved columns
190 (Fig 2, red) show a general increase during the summers due to increased volatilization rates.

191 The **Pasadena** site lies on the Northern edge of the Los Angeles conurbation in the United States of America, at
192 the foot of the San Gabriel mountains which rise steeply to the north to over 1.5 km altitude within 5 km
193 distance. Local sources of NH₃ include traffic, livestock, and occasional fires. FTIR observations typically take
194 place around local noon to avoid solar obstruction by nearby buildings and morning stratus cloud that is
195 common May-July. The highest retrieved columns (Fig.2, cyan) are observed during the summers.

196 The **Mexico City** site is located on the campus of the National Autonomous University of Mexico (UNAM) at
197 2280 m a.s.l., south of the metropolitan area. Surface NH₃ concentrations were measured by active open-path
198 FTIR during 2003 with typical values between 10 - 40 ppb (Moya et al. 2004). The megacity is host to more
199 than 22 million inhabitants, over 5 million motor vehicles and a wide variety of industrial activities. Low
200 ventilation during night and morning causes an effective accumulation of the NH₃ and other pollutants in
201 Mexico City, which is located in a flat basin surrounded by mountains. The concentration and vertical
202 distribution of pollutants are dominated by the large emissions and the dynamics of the boundary layer which is
203 on average 1.5 km height during the IASI morning overpass (Stremme et al., 2009, 2013). The retrieved
204 columns (Fig.2, orange) show an increase during the summers as well as a large daily variation.

205 The measurement site on the university campus of **St.-Denis** (Senten et al., 2008) is located on the remote
206 Reunion Island in the Indian Ocean. Observed NH₃ columns (Fig. 2, purple) are usually low due to the lack of
207 major sources nearby the site but increases are observed during the fire season (Sept.-Nov.) with possible fire
208 plumes originating from Madagascar, as already observed in another study involving short-lived species
209 (Vigouroux et al., 2009). Local NH₃ emissions include fertilizer applied for sugar cane production and local
210 biomass burning.

211 The **Wollongong** site is located on the campus of the University of Wollongong. The city of Wollongong is on
212 the south east coast of Australia with the University only about 2.5 km from the ocean. The measurement site is
213 also influenced by a 400m escarpment 1 km to the West, and the city of Sydney 60 km to the north. NH₃

214 sources come mainly from city traffic, as well as seasonal forest fires that can produce locally high amounts of
215 smoke and subsequent NH_3 emissions (Paton-Walsh et al., 2005). The retrieved columns (Fig.2, brown) peak
216 during the summer season due to the higher temperatures and seasonal forest fires.

217 The **Lauder** (Morgenstern et al., 2012) National Institute of Water and Atmospheric Research (NIWA) station
218 in Central Otago, New Zealand, is located in a hilly region with NH_3 emissions in the valley surrounding the
219 station mostly due to livestock grazing and fertilizer application. The observed columns (Fig. 2, black) show a
220 general increase during summers due to increased volatilization rates.

221

222

223 **2.3 FTIR and satellite comparison methodology**

224 **2.3.1 Co-location & data criteria**

225

226 NH₃ is highly variable in time and space which complicates the comparison between the IASI and FTIR
227 observations. Therefore collocation criteria were developed to investigate and mitigate the effect of the spatial
228 and temporal differences between the FTIR and IASI observations on their correlation. So far, there is no model
229 to describe the representativeness of a site for the region so a simple criterion was initially derived by analyzing
230 the terrain around each site and comparing the correlation of the IASI and FTIR observations for multiple time
231 and spatial differences to find the best correlation. To illustrate the differences between the representativeness of
232 the sites we take the stations at Bremen, Lauder and Wollongong as examples. Around Bremen the terrain is flat
233 with high reported NH₃ emissions (Kuenen et al., 2014) in the region surrounding the city. In contrast, Lauder is
234 located in a hilly region with low NH₃ emissions mostly due to local livestock grazing and fertilizer application
235 in the surrounding valleys (EDGAR, 2011). Owing to the flat terrain, the region around Bremen should, in
236 principle, have more homogeneous concentrations than Lauder. A more extreme case for geographical
237 inhomogeneity is Wollongong. Wollongong is located at the coast near a 400m escarpment without major
238 nearby NH₃ sources. Hence increasing distances between the satellite measurement pixel center and the station
239 may negatively impact the comparison due to the short lifetime of NH₃, and the limitation on transport of NH₃
240 to the site by the terrain (i.e. representativeness problems). Because no uniform criterion was found that would
241 enable a good comparison for all stations, multiple criteria with a maximum difference of between 10 km and 50
242 km will be used to analyze the optimal setting for each of the sites. Vertical sampling differences are not taken
243 into consideration in this study however the IASI selection criterion on the thermal contrast is conservative
244 and only those measurements for which IASI has a good sensitivity to surface concentrations are selected.

245

246 **Topography**

247 Any hill or mountain range located between the satellite pixel and the FTIR station may inhibit transport and
248 decrease their comparability. To account for the topography we only used observations that have at maximum
249 an altitude difference of 300 m (in) between the location of the FTIR and the IASI pixel position. The 300 m
250 criterion was chosen based on tests using the FTIR and satellite observations from Lauder. For the calculation of
251 the height differences we used the Space Shuttle Radar Topography Mission Global product at 3 arc second
252 resolution (SRTMGL3, Farr et al., 2007).

253

254 **Temporal variation**

255 NH₃ concentrations can vary considerably during the day, with lifetimes as short as a few hours not being
256 uncommon (Dentener and Crutzen, 1994; Bleeker et al., 2009). The variability of the concentrations mainly
257 arises from the variability in emission strengths as influenced by agricultural practices, meteorological, and
258 atmospheric conditions such as temperature, precipitation, wind speed and direction, the development of the
259 boundary layer (which is important as the IASI satellite observations take place around 9.30 local time and thus
260 the boundary layer has not always been fully established), pollution level, and deposition rates. To minimize the
261 effects of this variability on the comparability of the IASI and FTIR observations, satellite observations with a
262 time difference to FTIR observation of no more than 90 minutes were used.

263

264 **Product error**

265 The error of the IASI-NH₃ columns derives from errors on the HRI and the thermal contrast (Van Damme et al.,
266 2014a). Applying relative error filters of 50, 75 and 100% showed that mostly lower concentrations are removed
267 from the comparison. Consequently, introducing any criteria based on the associated (relative) error will bias
268 any comparison with FTIR columns towards the higher IASI total columns. Therefore, we decided not to filter
269 based on the relative error as it skews the range of NH₃ column totals.

270
271 **Meteorological factors**

272 The lowest detectable total column of the retrieval depends on the thermal contrast of the atmosphere (Van
273 Damme et al., 2014a). For example, the retrieval has a minimum detectable NH₃ column of around 5×10^{15}
274 molecules cm⁻² at a thermal contrast of about 12 Kelvin (K) for columns using the “transported” profile. A
275 thermal contrast of 12 K is chosen as the threshold to ensure the quality of the IASI observations, which
276 represents a lapse rate of around 8K/km altitude, near standard atmospheric conditions. We excluded data for
277 T_{skin} temperatures below 275.15 K to introduce a basic filter for snow cover and conditions with frozen soils.
278 The T_{skin} temperatures are obtained from the IASI L2 temperature profiles which have an uncertainty of ~2 K at
279 the surface (August et al., 2012). Finally, only IASI observations with a cloud cover below 10% are used.

280
281 The complete list of selection criteria is summarized in Table 2.

282
283 **Quality of the FTIR observations**

284 No filters were applied to maximize the number of observations usable in the comparison. The resolution and
285 detection limit of the FTIR instruments is usually better than that of the IASI instrument, leading to retrieved
286 columns with, in principle, less uncertainty. Overall the FTIR retrievals show an error of ~30% or less with the
287 largest errors due to the spectroscopic parameters (Dammers et al., 2015). While artefacts are possible in the
288 data we did not investigate for specific artefacts and possible impacts.

289
290
291 **2.3.2 Application of averaging kernels**

292 When performing a direct comparison between two remote sensing retrievals, one should take into account the
293 vertical sensitivity and the influence of a-priori profiles of both methods. One method to remove the influence of
294 the a-priori profile and the vertical sensitivity is the application of the averaging kernels of both retrievals to the
295 retrieved profiles of both products. The IASI-NH₃ HRI-based product scheme however, does not produce
296 averaging kernels thus it is not possible to account for the vertical sensitivity of the satellite retrieval. The effect
297 of the lack of the satellite averaging kernel is hard to predict, so the satellite vertical sensitivity is only taken into
298 account through the selection criterion on the thermal contrast. Nonetheless following the method described in
299 Rodgers and Connor (2003), the FTIR averaging kernel **A** is applied to the IASI profile x_{sat} to account for the
300 effects of the a-priori information and vertical sensitivity of the FTIR retrieval (the assumed profiles, called
301 “land” and “sea” are described in Van Damme et al., 2014a). The IASI profiles are not fully retrieved profiles
302 but fixed shape profiles used as an assumption in the IASI retrieval, see Van Damme et al., 2015a. These fixed
303 profiles are used for scaling purposes to be able to account for the FTIR averaging kernel. A total column

304 averaging kernel could be used instead, but in principle is similar to the procedure described here. The IASI
 305 profile is first mapped to the altitude grid of the FTIR profile by using interpolation, forming x_{sat}^{mapped} . Applying
 306 Eqn. (1), the smoothed IASI profile \hat{x}_{sat} is calculated indicating what the FTIR would retrieve when observing
 307 the satellite profile, which is then used to compute a total column. This profile can then be compared with the
 308 FTIR profile.

$$309 \quad \hat{x}_{sat} = x_{ftir}^{apriori} + A(x_{sat}^{mapped} - x_{ftir}^{apriori}) \quad (1)$$

310 After the application of the averaging kernel, for each FTIR observation, all satellite observations meeting the
 311 coincident criteria are averaged into a single mean total column value to be compared with the FTIR value. If
 312 multiple FTIR observations match a single satellite overpass, taking into account the maximum time difference,
 313 the FTIR observations are also averaged into a single mean total column value.

314

315 **3. Results**

316 **3.1 The influence of spatial differences between observations**

317

318 Following the approach of Irie et al. (2012) we will first show the correlation r , the slope as well as the mean
 319 relative difference (MRD) and the mean absolute difference (MAD) between satellite (y-axis) and FTIR NH₃
 320 total columns (x-axis) for each of the sites, as a function of the maximum allowable spatial difference between
 321 the observations (xdiff). The relative difference (RD) is defined here as,

322

$$323 \quad RD = \frac{(IASI \text{ column} - FTIR \text{ column}) \times 100}{FTIR \text{ column}} \quad (2)$$

324

325 A maximum relative difference of 200% was used to remove extreme outliers from the data, typically
 326 observations under wintertime conditions. The left side of Figure 3 shows the correlation coefficients (blue
 327 lines) and slope (red lines) for a selection of sites as a function of xdiff using a maximum allowed sampling time
 328 difference of 90 minutes. The right side of Figure 3 shows the MRD and MAD between the satellite and FTIR
 329 observations as a function of xdiff. The numbers on the bottom of each of the subfigures show the number of
 330 observations used in the comparison. The values in bold beside the title of each subplot give the mean
 331 concentrations of the IASI and FTIR observations. The bars indicate the standard deviation of the slope (left
 332 side figures) and the relative and absolute differences (right side figures).

333

334 For most stations an increasing xdiff (Figure 3) means a decreasing correlation (blue lines) and a changing slope
 335 (either decreasing or increasing with distance, red lines). This can be explained by the local character and high
 336 variation of NH₃ emissions/concentration in combination with the locations of the stations. Moving further away
 337 from a source will then generally decrease the relation between the concentration in the air and the emission
 338 source. The same is true for satellite observations of the air concentrations, which have a large footprint
 339 compared to the local character of a point measurement (FTIR) and the emissions. The steepness of this
 340 decrease (or increase) tells us something about the local variation in NH₃ concentrations, which can be large for

341 sites near heterogeneous emission sources or in cases with low transport/turbulence and thus overall relatively
342 low mixing.

343

344 Overall the highest correlations are seen at the Bremen site, which can partially be explained by the overall high
345 number of observations with high concentrations (more than $15\text{-}20 \times 10^{15}$ molecules cm^{-2}) which generally favours
346 the correlations. The mean column totals as well as the MRD and MAD do not change much except for the
347 smallest xdiff criteria. The larger changes for observations within 15 km are probably due to the smaller number
348 of observations (which follows from the relatively few IASI observations directly above or near the stations).
349 The results show an underestimation of observed columns by IASI with the “all stations” slopes in between
350 $\sim 0.6\text{-}0.8$. The stations with a lower mean FTIR column totals, such as Toronto and Boulder (as well as
351 Pasadena, Mexico City, and Lauder shown in the Appendix Figure A1) show lower correlations with most
352 having slopes below one. The correlations decreasing with mean column totals point towards the product
353 detection limits of the IASI- NH_3 product. The Toronto site has lower correlation coefficients for the smallest
354 xdiffs, but this seems to be due to the large drop in number of observations for a xdiff of <15 km. For higher
355 xdiff criteria the correlations of the Toronto site shows results similar to Bremen. The observations at Boulder
356 also show large differences when including more observations further away from the station. This can be
357 explained by the land use surrounding the Boulder site. Immediately west of the measurement site is a mountain
358 range which together with our elevation filter leads to rejection of the observations to the west. To the northeast
359 there are some major farming areas surrounding the river banks. Correlations do increase with a decreasing
360 xdiff, suggesting that IASI is able to resolve the large gradients in the NH_3 concentrations near the site.

361

362 From the correlation analysis as function of spatial coincidence, we conclude that a xdiff value of 25 km is
363 recommended to make a fair comparison between IASI- NH_3 and FTIR. Any criteria smaller than 15 km greatly
364 reduces the number of observations and statistics. xdiff beyond 25 km further decrease the correlations for the
365 combined set. From this point onward a xdiff value of 25 km will be used.

366

367 **3.2 Comparison of FTIR and IASI NH_3 data**

368 Observations from multiple years are used to show the coincident seasonal variability of the FTIR and IASI-
369 NH_3 products for each of the sites (Figure 4, FTIR: blue, IASI: red). Observations are grouped together into a
370 typical year as there are insufficient collocated observations to show an inter-annual time series. Note the
371 different scales on the y-axis. Similar seasonal cycles are clearly observed in both datasets for most stations.
372 Enhanced concentrations in spring are observed for Bremen and Toronto as well as Boulder due to manure
373 application. Most of the sites show an increase of NH_3 during the summer months which is likely due to the
374 increased volatilization of NH_3 as an effect of higher temperatures. Fire events that were earlier captured by
375 FTIR at St.-Denis in November, as well as in the IASI data, are not observed in the collocated sets, which is due
376 to a lack of coincident observations. Furthermore, there is a lack of observations in wintertime for most of the
377 stations either due to low thermal contrast or due to overcast conditions. Tsukuba has observations above the
378 detection limit but only one year of infrequent observations which is insufficient to show an entirely clear
379 seasonal cycle. A similar thing can be said for Pasadena where the number of coincident observations are too

380 few to make meaningful conclusions about the seasonal cycle. In conclusion, IASI reflects similar pollution
381 levels and seasonal cycles as deduced from the FTIR observations.

382

383 Figure 5 and 6 show a direct comparison of the FTIR and IASI NH_3 total columns for each station as well as a
384 combination of all the observations. Correlations, number of observations and slope are shown in the figures.
385 The MRD and these statistics are also summarized in Table 3. The comparison shows a variety of results. As
386 before, of all 9 stations Bremen shows the best correlation with a coefficient of determination of $r = 0.83$ and a
387 slope of 0.60. The intercept is not fixed at zero. The stations with overall lower observed total columns (less
388 than 10×10^{15} molecules cm^{-2}) show lower correlations. Stations with intermediate concentrations like Toronto
389 and Boulder show correlations $r = \sim 0.7-0.8$. The figure also shows the relatively low number of high
390 observations for both the FTIR and IASI values as a result of the relatively few FTIR observations during
391 events. The few outliers can have a disproportional effect on the slope as most of the lower observations are less
392 accurate due to the detection limits of the instruments. Overall most stations, except St.-Denis and Boulder and
393 Mexico City, indicate an underestimation by IASI of the FTIR columns ranging from 10-50%. The mean
394 relative differences for most stations are negative with most showing values in between $-22.5 \pm (54.0) \%$ for
395 Bremen down to a $-61.3 \pm (78.7) \%$ for St.-Denis. The bias shows some dependence on the total columns with
396 the underestimation being higher at stations with high mean total columns and lower at stations with low mean
397 total columns. An exception to this are stations with the lowest mean total columns (i.e. St.-Denis and
398 Wollongong). The differences at St.-Denis might be explained by the fact that most IASI observations are
399 positioned above water due to restrictions for terrain height differences. A similar thing can be said for
400 Wollongong which is situated on the coast with hills directly to the inland. Most observations are on the border
401 of water and land which might introduce errors in the retrieval. The combination of all observations gives a
402 MRD of $-32.4 \pm (56.3) \%$.

403

404 **4. Discussion and conclusions**

405

406 Recent satellite products enable the global monitoring of atmospheric concentrations of NH_3 . Unfortunately, the
407 validation of the satellite products of IASI (Van Damme et al., 2014a), TES (Shephard et al., 2011) and CrIS
408 (Shephard et al., 2015a) is very limited and, so far, only based on sparse in-situ and airborne studies. Dammers et
409 al. (2015) presented FTIR total column measurements of NH_3 at several places around the world and demonstrated
410 that these data can provide information about the temporal variation of the column concentrations, which are more
411 suitable for validation than ground-level concentrations. Ground-based remote sensing instruments have a long
412 history for validation of satellite products. FTIR observations are already commonly used for the validation of
413 many satellite products, including carbon monoxide (CO), methane (CH_4) and nitrous oxide (N_2O) (Wood et al.,
414 2002; Griesfeller et al., 2006; Dils et al., 2006; Kerzenmacher et al., 2012). Furthermore, MAX-DOAS systems
415 are used for the validation of retrievals for reactive gases (e.g. Irie et al., 2012), whereas AERONET is widely
416 used to validate satellite-derived aerosol optical depth (e.g. Schaap et al., 2008). The comparison between FTIR
417 and IASI NH_3 column reported here can be seen as a first step in the validation of NH_3 satellite products.

418

419 In this study, we collected FTIR measurements from nine locations around the world and followed the retrieval
420 described by Damers et al. (2015). The resulting datasets were used to quantify the bias and evaluate the
421 seasonal variability in the IASI-NH₃ product. Furthermore, we assessed the collocation criteria for the satellite
422 evaluation. Additional selection criteria based on thermal contrast, surface temperature, cloud cover and
423 elevation differences between observations, were applied to ensure the quality of the IASI-NH₃ observations.
424 The FTIR averaging kernels were applied to the satellite profiles to account for the vertical sensitivity of the
425 FTIR and the influence of the a-priori profiles.

426

427 To optimally compare the satellite product to the FTIR observations it is best to reduce the spatial collocation
428 criterion to the size of the satellite instrument's footprint and allow for a time difference as short as possible.
429 These considerations are to reduce effects of transport, chemistry and boundary layer growth but limit the
430 number of coinciding observations significantly. We have shown that the spatial distance between the IASI
431 observations and the FTIR measurement site is of importance: the larger the distance in space, the lower the
432 correlation. When there is no exact match in the position of both observations the variations in the spatial
433 separation lead to correlation coefficients that can greatly change even when changing the spatial criteria (xdiff)
434 from 10 to 30 km. Reasons for the changes are the local nature of NH₃ emissions, the surrounding terrain
435 characteristics and their influence on local transport of NH₃. The small values for spatial and temporal
436 coincidence criteria show the importance of NH₃ sources near the measurement sites when using these
437 observations for satellite validation. For the validation of the IASI observations, we used a xdiff of less than 25
438 km, which still showed high correlations while a large number of observations is retained for comparison.

439

440 Overall we see a broad consistency between the IASI and FTIR observations. The seasonal variations of both
441 datasets look similar for most stations. Increased column values are observed for both IASI and FTIR during
442 summers as the result of higher temperatures, with some sites showing an increase in concentrations due to
443 manure application and fertilization events in spring (Bremen, Toronto). In general our comparison shows that
444 IASI underestimates the NH₃ total columns, except for Wollongong. The Wollongong site has persistent low
445 background columns, i.e. observations with a low HRI, to which IASI is not very sensitive, which results in an
446 overestimation of the observed columns. Overall, correlations range from $r \sim 0.8$ for stations characterised by
447 higher NH₃ column totals (with FTIR columns up to 80×10^{15} molecules cm⁻²) to low $r \sim 0.4-0.5$ correlations for
448 stations, which only have a few to no FTIR observations above 5×10^{15} molecules cm⁻². Hence, the detection
449 limit or sensitivity of the IASI instrument largely explain the lower correlation values. The combination of all
450 sites ($N_{\text{obs}} = 547$) give a MRD of $-32.4 \pm (56.3) \%$, a correlation r of 0.8 with a slope of 0.73.

451

452 In comparison to ground-based in situ systems, the FTIR observations have the big advantage to provide coarse
453 vertical profiles, from which a column can be derived, which are more similar to what the satellite measures and
454 therefore more useful for validation. Dedicated NH₃ validation datasets are needed that better match the
455 overpass times of satellite instruments like IASI, TES and CrIS. This could be achieved by the addition of NH₃
456 to the NDACC measurement protocols and matching the overpass time of these satellites over these
457 measurement stations by using of the right spectral filters for detecting NH₃. Furthermore, the low number of
458 NDACC stations and their locations are not optimal for a dedicated validation of NH₃ satellite products.

459 Although these provide a starting point, the small set of stations does not cover the entire range of climate
460 conditions, agricultural source types and emission regimes. Hence, our validation results should be seen as
461 indicative. Additional stations or dedicated field campaigns are needed to improve this situation. New stations
462 should be placed in regions where emissions and geography are homogenous to ensure that stations are
463 representative for the footprints of the satellites. For validation of satellite products using FTIR measurements a
464 monitoring and measurements strategy needs to be developed with a representative mixture of locations in
465 addition to ground level data. The later can cover the spatial variation and different temporal measurements can
466 be used. The use of IASI and FTIR observations to study NH₃ distributions at ground level requires a
467 combination of model calculations and observations (e.g. Erisman et al., 2005a; 2005b). Such techniques are
468 required to provide all the necessary details to describe the high spatial and temporal variations in NH₃.

469
470 The direct comparison of the IASI and FTIR columns is an addition to earlier efforts by Van Damme et al.
471 (2015a) to validate IASI column observations with surface in situ and airborne observations. Our results
472 presented here indicate that the product performs better than the previously upper bound estimate of a factor 2
473 (i.e. -50 to +100%) as reported in Van Damme et al. (2014a). Although we tried to diminish any effect of
474 sampling time and position it cannot be ruled out completely that these impacts the comparison statistics as the
475 number of stations is small. Still the picture arising from the different stations is rather consistent, which hints at
476 other issues that may explain the observed bias. A number of important issues concerning the retrieval
477 techniques may explain the observed difference. First, the HRI based retrieval used for IASI is intrinsically
478 different to the optimal estimation based approach used for the FTIR retrieval. An IASI optimal estimation
479 retrieval for NH₃ called FORLI does exist but is not fully operationally used as it is computationally much
480 slower than the HRI method. Surprisingly a first comparison between the FORLI and HRI based retrieval (see
481 figure 9, Van Damme et al., 2014a) shows ~30% lower retrieved columns by the HRI scheme, which is very
482 close to the systematic difference quantified here. Do note that the results are not be fully comparable as the
483 reported HRI-FORLI comparison was for a limited dataset and no quality selection criteria were applied. We
484 recommend to further explore the use of the optimal estimation based IASI-NH₃ retrieval in comparison to the
485 FTIR observations. Second, the IASI and FTIR retrievals incorporate the same line spectroscopy database
486 (HITRAN 2012; Rothman et al., 2013) which removes a possible error due to different spectroscopy datasets.
487 The spectroscopy is the largest expected cause of error in the FTIR observations with measurement noise being
488 the close second for sites with low concentrations. An improvement to the line parameters (i.e. line intensity,
489 pressure and temperature effects) would greatly benefit both the FTIR and IASI retrievals. Thirdly, the HRI
490 based scheme uses the difference between spectra with and without the spectral signature of NH₃. A plausible
491 cause for error in this scheme is the influence and correlation of interfering species in the same spectral
492 channels. H₂O lines occur near most of the NH₃ spectral lines and interfere with the NH₃ lines at the resolution
493 of the IASI instrument. Humidity levels vary throughout the year with an increase amount of water vapour in
494 summer conditions. The HRI based scheme uses a fixed amount of water vapour and varying amounts of water
495 vapour may interfere with the HRI value attributed fully to the NH₃ columns. As there is a seasonality in the
496 water vapour content of the atmosphere (Wagner et al., 2006), any error attributed to water vapour should show
497 a seasonality in the difference between the IASI and FTIR observations. A seasonality was, however, not visible
498 although it may be that the number of coincident observations was too small to recognize it. This again shows

499 the need for dedicated NH₃ validation data (e.a. dedicated FTIR observations). Fourth, the negative bias of the
500 satellite observations can be expected by the lack of sensitivity to concentrations near the surface. This is of
501 course where the ammonia concentrations usually peak. The FTIR observations however do fully observe the
502 lower layers in the troposphere thus causing a discrepancy. Normally one can correct for this using the
503 averaging kernel of the satellite observations. However, the IASI-NH₃ retrieval does not produce an averaging
504 kernel meaning it is not possible to calculate the exact effect. The use of a typical averaging kernel will cause
505 more uncertainty as there is a large day to day variability in the averaging kernels as earlier retrievals showed
506 (Clarisse et al., 2009). Finally, another possible cause of error is the lack of a varying NH₃ profile and the proxy
507 used for thermal contrast to describe the state of the atmosphere. The sensitivity of the scheme to the
508 concentrations of NH₃ in the boundary layer is described by using a fixed profile for land and sea observations
509 in combination with a thermal contrast based on two layers (surface and 1.5 km) as it is expected that most of
510 the NH₃ occurs in the boundary layer. In reality the NH₃ profile is highly dynamic due to a varying boundary
511 layer height and changing emissions as well as temperature changes (e.g. inversions etc) occurring throughout
512 the planetary boundary layer. Not accounting for this can introduce an error and future HRI based schemes
513 should focus on estimating the possible effects of using only a specific profile. The use of multiple NH₃-profiles
514 in combination with multiple temperature layers would be a better approximation of state of the atmosphere,
515 although computationally more expensive. The sharp difference between the sea and land retrieval introduces
516 strong variability in observations near the coast. Furthermore, observations that are directly on the transition
517 between water and land can introduce problems due to the varying emissivity. Similar issues have been reported
518 for aerosol retrievals (e.g. Schaap et al., 2008).

519
520 Although the FTIR observations offer some vertical information, studies combining this technique with tower or
521 airborne observations are needed to further improve knowledge and sensitivity of the FTIR and satellite
522 observations to the vertical distribution of NH₃. Without this knowledge, it is not possible to use the
523 observations for quantitative emission estimates and modelling purposes as no uncertainty on the new estimate
524 can be given. Approaches similar to the recent study by Shephard et al. (2015b) using an airborne instrument,
525 possibly in combination with an FTIR system focused on the overpass of multiple satellite systems for an
526 extended period of time should be used to establish the sensitivities and biases of the different retrieval products
527 available from satellite instruments as well as the bias between the satellite and surface instruments. The use of
528 IASI and FTIR observations to study NH₃ distributions at ground level requires a combination of model
529 calculations and observations. Such techniques are required to provide all the necessary details to describe the
530 high spatial and temporal variations in NH₃.

531

532 **Acknowledgements**

533 This work is part of the research programme GO/12-36, which is financed by the Netherlands Organisation for
534 Scientific Research (NWO). The Lauder NIWA FTIR program is funded through the New Zealand
535 government's core research grant framework from the Ministry of Business, Innovation and employment. We
536 thank the Lauder FTIR team for their contribution. Acknowledgements are addressed to the Université de La
537 Réunion and CNRS (LACy-UMR8105 and UMS3365) for their support of the Reunion Island measurements.
538 The Reunion Island data analysis has mainly been supported by the A3C project (PRODEX Program of the

539 Belgian Science Policy Office, BELSPO, Brussels). The University of Toronto's NDACC contribution has been
540 supported by the CAFTON project, funded by the Canadian Space Agency's FAST Program. Measurements
541 were made at the University of Toronto Atmospheric Observatory (TAO), which has been supported by
542 CFCAS, ABB Bomem, CFI, CSA, EC, NSERC, ORDCF, PREA, and the University of Toronto. Part of this
543 research was performed at the Jet Propulsion Laboratory, California Institute of Technology, under contract with
544 NASA. IASI has been developed and built under the responsibility of the "Centre national d'études spatiales"
545 (CNES, France). It is flown on-board the Metop satellites as part of the EUMETSAT Polar System. The IASI
546 L1 data are received through the EUMETCast near real-time data distribution service.
547 The IASI-related activities in Belgium were funded by Belgian Science Policy Office through the IASI.Flow
548 Prodex arrangement (2014-2018). PFC, LC and MVD also thank the FRS-FNRS for financial support. L.C. is a
549 research associate with the Belgian F.R.S-FNRS. C. Clerbaux is grateful to CNES for scientific collaboration
550 and financial support. The National Center for Atmospheric Research is supported by the National Science
551 Foundation. The Boulder observation program is supported in part by the Atmospheric Chemistry Observations
552 & Modeling Division of NCAR. The measurement programme and NDACC site at Wollongong has been
553 supported by the Australian Research Council for many years, most recent by grant DP110101948 and
554 LE0668470. The Mexico City site was funded through projects UNAM-DGAPA (109914) and CONACYT
555 (249374, 239618). A. Bezanilla, J. Baylón and E. Plaza are acknowledged for their participation in the
556 measurements and analysis. We would like to thank David Griffith, Clare Murphy and Voltaire Velazco at the
557 School of Chemistry, University of Wollongong, for maintaining FTS instrumentation and conducting FTS
558 measurements. We are grateful to the many colleagues who have contributed to FTIR data acquisition at the
559 various sites.

560

561 **References**

562

563 Adams, P.J., Seinfeld, J.H., Koch, D., Mickley, L., Jacob, D. (2001), General circulation model assessment of
564 direct radiative forcing by the sulfate-nitrate-ammonium-water inorganic aerosol system, *Journal of Geophysical*
565 *Research Atmospheres*, 106 (1), pp. 1097-1111.

566

567 August, T., Klaes, D., Schlüssel, P., Hultberg, T., Crapeau, M., Arriaga, A., O'Carroll, A., Coppens, D., Munro,
568 R. and Calbet, X.: IASI on Metop-A: Operational Level 2 retrievals after five years in orbit, *J. Quant. Spectrosc.*
569 *Radiat. Transf.*, 113(11), 1340–1371, doi:10.1016/j.jqsrt.2012.02.028, 2012.

570

571 Beer, R., Shephard, M. W., Kulawik, S. S., Clough, S. a., Eldering, A., Bowman, K. W., Sander, S. P., Fisher, B.
572 M., Payne, V. H., Luo, M., Osterman, G. B. and Worden, J. R.: First satellite observations of lower tropospheric
573 ammonia and methanol, *Geophys. Res. Lett.*, 35(9), 1–5, doi:10.1029/2008GL033642, 2008.

574

575 Bleeker, A., Sutton, M. A., Acherman, B., Alebic-Juretic, A., Aneja, V. P., Ellermann, T., Erisman, J. W., Fowler,
576 D., Fagerli, H., Gauger, T., Harlen, K. S., Hole, L. R., Horvath, L., Mitisinkova, M., Smith, R. I., Tang, Y. S.,
577 and Pul, A.: Linking ammonia emission trends to measured concentrations and deposition of reduced nitrogen at
578 different scales, in: *Atmospheric Ammonia – Detecting emission changes and environmental impacts. Results of*
579 *an expert workshop under the convention of long-range transboundary air pollution*, edited by: Sutton M. A., Reis
580 S., Baker S. M. H. , *Atmospheric Ammonia – Detecting emission changes and environmental impacts. Results of*
581 *an expert workshop under the convention of long-range transboundary air pollution*, Springer, 123–180, 2009.

582

583 Bobbink, R, Hicks K, Galloway J, Spranger T, Alkemade R, Ashmore M, Bustamante M, Cinderby S, Davidson
584 E, Dentener F, Emmett B, Erisman JW, Fenn M, Gilliam F, Nordin A, Pardo L, De Vries W. Global assessment
585 of nitrogen deposition effects on terrestrial plant diversity: a synthesis, *Ecological Applications*, 20 (2010), pp.
586 30–59.

587

588 von Bobruzki, K., Braban, C. F., Famulari, D., Jones, S. K., Blackall, T., Smith, T. E. L., Blom, M., Coe, H.,
589 Gallagher, M., Ghalaieny, M., McGillen, M. R., Percival, C. J., Whitehead, J. D., Ellis, R., Murphy, J.,
590 Mohacsi, A., Pogany, A., Junninen, H., Rantanen, S., Sutton, M. A., and Nemitz, E.: Field inter-comparison of
591 eleven atmospheric ammonia measurement techniques, *Atmos. Meas. Tech.*, 3, 91-112, doi:10.5194/amt-3-91-
592 2010, 2010.

593 Brown, L. R., M. R. Gunson, R. A. Toth, F. W. Irion, C. P. Rinsland, and A. Goldman. "1995 atmospheric trace
594 molecule spectroscopy (ATMOS) linelist." *Applied optics* 35, no. 16 (1996): 2828-2848.

595 Chang, L., Palo, S., Hagan, M., Richter, J., Garcia, R., Riggan, D. and Fritts, D.: Structure of the migrating diurnal
596 tide in the Whole Atmosphere Community Climate Model (WACCM), *Advances in Space Research*, 41(9), 1398–
597 1407, doi:10.1016/j.asr.2007.03.035, 2008.

598 Coheur, P.-F., Clarisse, L., Turquety, S., Hurtmans, D., and Clerbaux, C.: IASI measurements of reactive trace
599 species in biomass burning plumes, *Atmos. Chem. Phys.*, 9, 5655-5667, doi:10.5194/acp-9-5655-2009, 2009.

600 Clarisse, Lieven, Cathy Clerbaux, Frank Dentener, Daniel Hurtmans, and Pierre-François Coheur. "Global
601 ammonia distribution derived from infrared satellite observations." *Nature Geoscience* 2, no. 7 (2009): 479-483.

602 Clarisse, L., Shephard, M. W., Dentener, F., Hurtmans, D., Cady-Pereira, K., Karagulian, F., Van Damme, M.,
603 Clerbaux, C. and Coheur, P.-F.: Satellite monitoring of ammonia: A case study of the San Joaquin Valley, *J.*
604 *Geophys. Res.*, 115(D13), 1–15, doi:10.1029/2009JD013291, 2010.

605 Dammers, E., Vigouroux, C., Palm, M., Mahieu, E., Warneke, T., Smale, D., Langerock, B., Franco, B., Van
606 Damme, M., Schaap, M., Notholt, J., and Erisman, J. W.: Retrieval of ammonia from ground-based FTIR solar
607 spectra, *Atmos. Chem. Phys.*, 15, 12789-12803, doi:10.5194/acp-15-12789-2015, 2015.

608 Dentener, F. J. and Crutzen, P. J.: A three-dimensional model of the global ammonia cycle, *J. Atmos. Chem.*,
609 19(4), 331–369, doi:10.1007/BF00694492, 1994.

610 Dentener, F., Drevet, J., Lamarque, J. F., Bey, I., Eickhout, B., Fiore, A. M., Hauglustaine, D., Horowitz, L. W.,
611 Krol, M., Kulshrestha, U. C., Lawrence, M., Galy-Lacaux, C., Rast, S., Shindell, D., Stevenson, D., Van Noije,
612 T., Atherton, C., Bell, N., Bergman, D., Butler, T., Cofala, J., Collins, B., Doherty, R., Ellingsen, K., Galloway,
613 J., Gauss, M., Montanaro, V., Müller, J. F., Pitari, G., Rodriguez, J., Sanderson, M., Solmon, F., Strahan, S.,

614 Schultz, M., Sudo, K., Szopa, S. and Wild, O.: Nitrogen and sulfur deposition on regional and global scales: A
615 multimodel evaluation, *Global Biogeochem. Cycles*, 20(4), doi:10.1029/2005GB002672, 2006.
616
617
618 Dils, B., De Mazière, M., Müller, J. F., Blumenstock, T., Buchwitz, M., de Beek, R., Demoulin, P., Duchatelet, P.,
619 Fast, H., Frankenberg, C., Gloudemans, A., Griffith, D., Jones, N., Kerzenmacher, T., Kramer, I., Mahieu, E.,
620 Mellqvist, J., Mittermeier, R. L., Notholt, J., Rinsland, C. P., Schrijver, H., Smale, D., Strandberg, A.,
621 Straume, A. G., Stremme, W., Strong, K., Sussmann, R., Taylor, J., van den Broek, M., Velasco, V., Wagner, T.,
622 Warneke, T., Wiacek, A., and Wood, S.: Comparisons between SCIAMACHY and ground-based FTIR data for
623 total columns of CO, CH₄, CO₂ and N₂O, *Atmos. Chem. Phys.*, 6, 1953-1976, doi:10.5194/acp-6-1953-2006,
624 2006.

625 EDGAR-Emission Database for Global Atmospheric Research: Source: EC-JRC/PBL. EDGAR version 4.2.,
626 <http://edgar.jrc.ec.europa.eu>, access 15th October 2012, 2011
627

628 Erisman, J. W., Hensen, A., Mosquera, J., Sutton, M. and Fowler, D.: Deposition monitoring networks: what
629 monitoring is required to give reasonable estimates of ammonia/ammonium?, *Environ. Pollut.*, 135(3), 419–431,
630 doi:<http://dx.doi.org/10.1016/j.envpol.2004.11.015>, 2005a.
631

632 Erisman, J. W., Vermeulen, A., Hensen, A., Flechard, C., Dämmgen, U., Fowler, D., Sutton, M., Grünhage, L.
633 and Tuovinen, J. P.: Monitoring and modelling of biosphere/atmosphere exchange of gases and aerosols in
634 Europe, *Environ. Pollut.*, 133(3), 403–413, doi:10.1016/j.envpol.2004.07.004, 2005b.
635

636 Erisman, J. W., Bleeker, a., Galloway, J. and Sutton, M. S.: Reduced nitrogen in ecology and the environment,
637 *Environ. Pollut.*, 150(1), 140–149, doi:10.1016/j.envpol.2007.06.033, 2007.
638

639 Erisman, J. W., Sutton, M. a., Galloway, J., Klimont, Z. and Winiwarter, W.: How a century of ammonia synthesis
640 changed the world, , 1(October 1908), doi:10.1038/ngeo325, 2008.
641

642 Erisman, J. W., Galloway, J., Seitzinger, S., Bleeker, A. and Butterbach-Bahl, K.: Reactive nitrogen in the
643 environment and its effect on climate change, *Curr. Opin. Environ. Sustain.*, 3(5), 281–290,
644 doi:10.1016/j.cosust.2011.08.012, 2011.
645

646 Farr, T. G., Rosen, P. a., Caro, E. and Crippen, R.: The Shuttle Radar Topography Mission, *Rev. ...*, (2005), 1–
647 33, doi:10.1029/2005RG000183.1.INTRODUCTION, 2007.
648

649 Fowler, D., Coyle, M., Skiba, U., Sutton, M. A., Cape, J. N., Reis, S., Sheppard, L. J., Jenkins, A., Grizzetti, B.,
650 Galloway, J. N., Vitousek, P., Leach, A., Bouwman, A. F., Butterbach-Bahl, K., Dentener, F., Stevenson, D.,
651 Amann, M. and Voss, M.: The global nitrogen cycle in the twenty-first century, *Philos. Trans. R. Soc. London B*
652 *Biol. Sci.*, 368(1621) [online] Available from:
653 <http://rstb.royalsocietypublishing.org/content/368/1621/20130164.abstract>, 2013.
654

655 Griesfeller, a., Griesfeller, J., Hase, F., Kramer, I., Loës, P., Mikuteit, S., Raffalski, U., Blumenstock, T. and
656 Nakajima, H.: Comparison of ILAS-II and ground-based FTIR measurements of O₃, HNO₃, N₂O, and CH₄
657 over Kiruna, Sweden, *J. Geophys. Res.*, 111(D11), D11S07, doi:10.1029/2005JD006451, 2006.
658

659 Hase, F., Blumenstock, T. and Paton-Walsh, C.: Analysis of the instrumental line shape of high-resolution
660 fourier transform IR spectrometers with gas cell measurements and new retrieval software., *Appl. Opt.*, 38(15),
661 3417–3422, 1999.
662

663 Hase, F., Hannigan, J. W., Coffey, M. T., Goldman, a., Höpfner, M., Jones, N. B., Rinsland, C. P. and Wood, S.
664 W.: Intercomparison of retrieval codes used for the analysis of high-resolution, ground-based FTIR
665 measurements, *J. Quant. Spectrosc. Radiat. Transf.*, 87(1), 25–52, doi:10.1016/j.jqsrt.2003.12.008, 2004.
666

667 Hase, F., Demoulin, P., Sauval, A. J., Toon, G. C., Bernath, P. F., Goldman, A., Hannigan, J. W., Rinsland, C. P.:
668 An empirical line-by-line model for the infrared solar transmittance spectrum from 700 to 5000 cm⁻¹, *J. Quant.*
669 *Spectrosc. Ra.*, 102, 450–463, doi:10.1016/j.jqsrt.2006.02.026, 2006.
670

671 Holland, E. a., Dentener, F. J., Braswell, B. H. and Sulzman, J. M.: Contemporary and pre-industrial global
672 reactive nitrogen budgets, *Biogeochemistry*, 46(1-3), 7–43, doi:10.1007/BF01007572, 1999.

673
674 Irie, H., Boersma, K. F., Kanaya, Y., Takashima, H., Pan, X. and Wang, Z. F.: Quantitative bias estimates for
675 tropospheric NO₂ columns retrieved from SCIAMACHY, OMI, and GOME-2 using a common standard for
676 East Asia, *Atmos. Meas. Tech.*, 5(10), 2403–2411, doi:10.5194/amt-5-2403-2012, 2012.
677
678 Kerzenmacher, T., Dils, B., Kumps, N., Blumenstock, T., Clerbaux, C., Coheur, P.-F., Demoulin, P., García, O.,
679 George, M., Griffith, D. W. T., Hase, F., Hadji-Lazaro, J., Hurtmans, D., Jones, N., Mahieu, E., Notholt, J., Paton-
680 Walsh, C., Raffalski, U., Ridder, T., Schneider, M., Servais, C., and De Mazière, M.: Validation of IASI FORLI
681 carbon monoxide retrievals using FTIR data from NDACC, *Atmos. Meas. Tech.*, 5, 2751–2761, doi:10.5194/amt-
682 5-2751-2012, 2012.
683
684
685 Leen, J. B., Yu, X. Y., Gupta, M., Baer, D. S., Hubbe, J. M., Kluzek, C. D., Tomlinson, J. M. and Hubbell, M. R.:
686 Fast in situ airborne measurement of ammonia using a mid-infrared off-axis ICOS spectrometer, *Environ. Sci.*
687 *Technol.*, 47(18), 10446–10453, doi:10.1021/es401134u, 2013.
688
689 Luo, M., Shephard, M. W., Cady-Pereira, K. E., Henze, D. K., Zhu, L., Bash, J. O., Pinder, R. W., Capps, S. L.,
690 Walker, J. T. and Jones, M. R.: Satellite observations of tropospheric ammonia and carbon monoxide: Global
691 distributions, regional correlations and comparisons to model simulations, *Atmos. Environ.*, 106, 262–277,
692 doi:10.1016/j.atmosenv.2015.02.007, 2015.
693
694 Lutsch, E., Damers, E., Conway, S. and Strong, K: Ground-based FTIR measurements of CO, HCN, C₂H₆ and
695 NH₃ emissions from the 2014 Canadian Wildfires, *in preparation*.
696
697 Morgenstern, O., Zeng, G., Wood, S. W., Robinson, J., Smale, D., Paton-Walsh, C., Jones, N. B., and Griffith,
698 D. W. T.: Long-range correlations in Fourier transform infrared, satellite, and modeled CO in the Southern
699 Hemisphere, *J. Geophys. Res.*, 117, D11301 doi:10.1029/2012JD017639, 2012.
700
701 Moya, M., Fountoukis, C., Nenes, A., Matías, E., and Grutter, M.: Predicting diurnal variability of fine
702 inorganic aerosols and their gas-phase precursors near downtown Mexico City, *Atmos. Chem. Phys. Discuss.*, 7,
703 11257–11294, doi:10.5194/acpd-7-11257-2007, 2007.
704
705 Nowak, J. B., Neuman, J. A., Kozai, K., Huey, L. G., Tanner, D. J., Holloway, J. S., Ryerson, T. B., Frost, G. J.,
706 McKeen, S. A., and Fehsenfeld, F. C.: A chemical ionization mass spectrometry technique for airborne
707 measurements of ammonia, *J. Geophys. Res.-Atmos.*, 112, D10S02, doi:10.1029/2006JD007589, 2007.
708
709 Nowak, J. B., Neuman, J. A., Bahreini, R., Brock, C. A., Middlebrook, A. M., Wollny, A. G., Holloway, J. S.,
710 Peischl, J., Ryerson, T. B., and Fehsenfeld, F. C.: Airborne observations of ammonia and ammonium nitrate
711 formation over Houston, Texas, *J. Geophys. Res.-Atmos.*, 115, D22 304, doi:10.1029/ 2010JD014195, 2010.
712
713 Ohyama, H., Morino, I., Nagahama, T., Machida, T., Suto, H., Oguma, H., Sawa, Y., Matsueda, H., Sugimoto,
714 N., Nakane, H., and Nakagawa, K.: Column-averaged volume mixing ratio of CO₂ measured with ground-based
715 Fourier transform spectrometer at Tsukuba, *J. Geophys. Res.*, 114, D18303, doi:10.1029/2008JD011465, 2009.
716
717 Paton-Walsh, C., Jones, N. B., Wilson, S. R., Haverd, V., Meier, A., Griffith, D. W. T. and Rinsland, C. P.
718 (2005), Measurements of trace gas emissions from Australian forest fires and correlations with coincident
719 measurements of aerosol optical depth, *J. Geophys. Res.*, 110, D24305, doi:24310.21029/22005JD006202
720
721 Pope, III, C. A., Ezzati, M., and Dockery, D. W.: Fine-Particulate Air Pollution and Life Expectancy in the United
722 States, *N. Engl. J. Med.*, 360, 376–386, doi:{10.1056/NEJMsa0805646}, 2009.
723
724 Pougatchev, N. S., Connor, B. J., & Rinsland, C. P. (1995). Infrared measurements of the ozone vertical
725 distribution above Kitt Peak. *Journal of Geophysical Research: Atmospheres (1984–2012)*, 100(D8), 16689-
726 16697.
727
728 Puchalski, M. A., M. E. Sather, J. T. Walker, C. M. Lehmann, D. A. Gay, J. Mathew, and W. P. Robarge (2011),
729 Passive ammonia monitoring in the United States: Comparing three different sampling devices, *J. Environ. Monit.*,
730 13(11), 3156–3167, doi:10.1039/c1em10553a.
731

732 Ravishankara, A. R., Daniel, J. S. and Portmann, R. W.: Nitrous oxide (N₂O): the dominant ozone-depleting
733 substance emitted in the 21st century., *Science*, 326(5949), 123–125, doi:10.1126/science.1176985, 2009.
734

735 Rockstrom, J., Steffen, W., Noone, K., Persson, A., Chapin, F. S., Lambin, E. F., Lenton, T. M., Scheffer, M.,
736 Folke, C., Schellnhuber, H. J., Nykvist, B., de Wit, C. A., Hughes, T., van der Leeuw, S., Rodhe, H., Sorlin, S.,
737 Snyder, P. K., Costanza, R., Svedin, U., Falkenmark, M., Karlberg, L., Corell, R. W., Fabry, V. J., Hansen, J.,
738 Walker, B., Liverman, D., Richardson, K., Crutzen, P. and Foley, J. A.: A safe operating space for humanity,
739 *Nature*, 461(7263), 472–475 [online] Available from: <http://dx.doi.org/10.1038/461472a>, 2009.
740

741 Rodgers, C. D.: *Inverse Methods for Atmospheric Sounding - Theory and Practice*, 2(January), 256,
742 doi:10.1142/9789812813718, 2000.
743

744 Rodgers, C. D. and Connor, B. J.: Intercomparison of remote sounding instruments, *J. Geophys. Res. Atmos.*,
745 108(D3), n/a–n/a, doi:10.1029/2002JD002299, 2003.
746

747 Rodhe, Henning, Frank Dentener, and Michael Schulz. "The global distribution of acidifying wet
748 deposition." *Environmental Science & Technology* 36.20 (2002): 4382-4388.
749

750 Rothman, L. S., Gordon, I. E., Babikov, Y., Barbe, a., Chris Benner, D., Bernath, P. F., Birk, M., Bizzocchi, L.,
751 Boudon, V., Brown, L. R., Campargue, a., Chance, K., Cohen, E. a., Coudert, L. H., Devi, V. M., Drouin, B. J.,
752 Fayt, a., Flaud, J. M., Gamache, R. R., Harrison, J. J., Hartmann, J. M., Hill, C., Hodges, J. T., Jacquemart, D.,
753 Jolly, a., Lamouroux, J., Le Roy, R. J., Li, G., Long, D. a., Lyulin, O. M., Mackie, C. J., Massie, S. T.,
754 Mikhailenko, S., Müller, H. S. P., Naumenko, O. V., Nikitin, a. V., Orphal, J., Perevalov, V., Perrin, a.,
755 Polovtseva, E. R., Richard, C., Smith, M. a H., Starikova, E., Sung, K., Tashkun, S., Tennyson, J., Toon, G. C.,
756 Tyuterev, V. G. and Wagner, G.: The HITRAN2012 molecular spectroscopic database, *J. Quant. Spectrosc.*
757 *Radiat. Transf.*, 130, 4–50, doi:10.1016/j.jqsrt.2013.07.002, 2013.
758

759 Schaap, M., van Loon, M., ten Brink, H. M., Dentener, F. J., and Bultjes, P. J. H.: Secondary inorganic aerosol
760 simulations for Europe with special attention to nitrate, *Atmos. Chem. Phys.*, 4, 857-874, doi:10.5194/acp-4-857-
761 2004, 2004
762

763 Schaap, M., Timmermans, R. M. a, Koelemeijer, R. B. a, de Leeuw, G. and Bultjes, P. J. H.: Evaluation of
764 MODIS aerosol optical thickness over Europe using sun photometer observations, *Atmos. Environ.*, 42(9), 2187–
765 2197, doi:10.1016/j.atmosenv.2007.11.044, 2008.
766

767 Senten, C., De Mazière, M., Dils, B., Hermans, C., Kruglanski, M., Neefs, E., Scolas, F., Vandaele, A. C.,
768 Vanhaelewyn, G., Vigouroux, C., Carleer, M., Coheur, P. F., Fally, S., Barret, B., Baray, J. L., Delmas, R., Leveau,
769 J., Metzger, J. M., Mahieu, E., Boone, C., Walker, K. A., Bernath, P. F., and Strong, K.: Technical Note: New
770 ground-based FTIR measurements at Ile de La Réunion: observations, error analysis, and comparisons with
771 independent data, *Atmos. Chem. Phys.*, 8, 3483-3508, doi:10.5194/acp-8-3483-2008, 2008.
772

773 Shephard, M. W., Cady-Pereira, K. E., Luo, M., Henze, D. K., Pinder, R. W., Walker, J. T., Rinsland, C. P.,
774 Bash, J. O., Zhu, L., Payne, V. H., and Clarisse, L.: TES ammonia retrieval strategy and global observations of
775 the spatial and seasonal variability of ammonia, *Atmos. Chem. Phys.*, 11, 10743-10763, doi:10.5194/acp-11-
776 10743-2011, 2011.

777 Shephard, M. W. and Cady-Pereira, K. E.: Cross-track Infrared Sounder (CrIS) satellite observations of
778 tropospheric ammonia, *Atmos. Meas. Tech.*, 8, 1323-1336, doi:10.5194/amt-8-1323-2015, 2015a.

779 Shephard, M. W., McLinden, C. A., Cady-Pereira, K. E., Luo, M., Moussa, S. G., Leithead, A., Liggio, J., Staebler,
780 R. M., Akingunola, A., Makar, P., Lehr, P., Zhang, J., Henze, D. K., Millet, D. B., Bash, J. O., Zhu, L., Wells, K.
781 C., Capps, S. L., Chaliyakunnel, S., Gordon, M., Hayden, K., Brook, J. R., Wolde, M., and Li, S.-M.: Tropospheric
782 Emission Spectrometer (TES) satellite validations of ammonia, methanol, formic acid, and carbon monoxide over
783 the Canadian oil sands, *Atmos. Meas. Tech. Discuss.*, 8, 9503-9563, doi:10.5194/amtd-8-9503-2015, 2015b.

784 Slanina, J., ten Brink, H. M., Otjes, R. P., Even, A., Jongejan, P., Khlystov, A., Waijers-Ijpelaar, A., Hu, M., and
785 Lu, Y.: Continuous analysis of nitrate and ammonium in aerosols by the Steam Jet Aerosol Collector (SJAC),
786 *Atmos. Environ.*, 35, 2319–2330, 2001.

877 Stremme, W., Ortega, I., and Grutter, M.: Using ground-based solar and lunar infrared spectroscopy to study the
878 diurnal trend of carbon monoxide in the Mexico City boundary layer, *Atmos. Chem. Phys.*, 9, 8061-8078,
879 doi:10.5194/acp-9-8061-2009, 2009.

790 Stremme, W., Grutter, M., Rivera, C., Bezanilla, A., Garcia, A. R., Ortega, I., George, M., Clerbaux, C., Coheur,
791 P.-F., Hurtmans, D., Hannigan, J. W., and Coffey, M. T.: Top-down estimation of carbon monoxide emissions
792 from the Mexico Megacity based on FTIR measurements from ground and space, *Atmos. Chem. Phys.*, 13, 1357-
793 1376, doi:10.5194/acp-13-1357-2013, 2013.

794 Sutton, M., Stefan Reis, and Samantha MH Baker. "Atmospheric ammonia." *Detecting Emission Changes and*
795 *Environmental Impacts* 494 (2009).

796 Sutton, M. a, Reis, S., Riddick, S. N., Dragosits, U., Nemitz, E., Theobald, M. R., Tang, Y. S., Braban, C. F.,
797 Vieno, M., Dore, A. J., Mitchell, R. F., Wanless, S., Daunt, F., Fowler, D., Blackall, T. D., Milford, C., Flechard,
798 C. R., Loubet, B., Massad, R., Cellier, P., Personne, E., Coheur, P. F., Clarisse, L., Van Damme, M., Ngadi, Y.,
799 Clerbaux, C., Skjøth, C. A., Geels, C., Hertel, O., Wichink Kruit, R. J., Pinder, R. W., Bash, J. O., Walker, J. T.,
800 Simpson, D., Horváth, L., Misselbrook, T. H., Bleeker, A., Dentener, F. and de Vries, W.: Towards a climate-
801 dependent paradigm of ammonia emission and deposition., *Philos. Trans. R. Soc. Lond. B. Biol. Sci.*, 368(1621),
802 20130166, doi:10.1098/rstb.2013.0166, 2013.

803 Sun, K., Cady-Pereira, K., Miller, D. J. , Tao, L., Zondlo, M.A. , Nowak, J. B., Neuman, J. A., Mikoviny, T.,
804 Müller, M. , Wisthaler, A., Scarino, A. J., and Hostetler, C. A.: Validation of TES ammonia observations at the
805 single pixel scale in the San Joaquin Valley during DISCOVER-AQ, *J. Geophys. Res.-Atmos.*, 120, 5140–5154,
806 doi:10.1002/2014JD022846, 2015.

807
808 Toon, G. C., Blavier, J.-F., Sen, B., Margitan, J. J., Webster, C. R., Max, R. D., Fahey, D. W., Gao, R., DelNegro,
809 L., Proffitt, M., Elkins, J., Romashkin, P. A., Hurst, D. F., Oltmans, S., Atlas, E., Schauffler, S., Flocke, F., Bui,
810 T. P., Stimpfle, R. M., Bonne, G. P., Voss, P. B., and Cohen, R. C.: Comparison of MkIV balloon and ER-2
811 aircraft measurements of atmospheric trace gases, *J. Geophys. Res.*, 104, 26 779–26 790, 1999.

812
813 Van Damme, M., Clarisse, L., Heald, C. L., Hurtmans, D., Ngadi, Y., Clerbaux, C., Dolman, A. J., Erisman, J. W.,
814 and Coheur, P. F.: Global distributions, time series and error characterization of atmospheric ammonia (NH₃) from
815 IASI satellite observations, *Atmos. Chem. Phys.*, 14, 2905-2922, doi:10.5194/acp-14-2905-2014, 2014a.

816
817 Van Damme, M., R. J. Wichink Kruit, M. Schaap, L. Clarisse, C. Clerbaux, P.-F. Coheur, E. Dammers, A. J.
818 Dolman, and J. W. Erisman , Evaluating 4 years of atmospheric ammonia (NH₃) over Europe using IASI satellite
819 observations and LOTOS-EUROS model results, *J. Geophys. Res. Atmos.*, 119, 9549–9566,
820 doi:10.1002/2014JD021911, 2014b.

821
822 Van Damme, M., Clarisse, L., Dammers, E., Liu, X., Nowak, J. B., Clerbaux, C., Flechard, C. R., Galy-Lacaux,
823 C., Xu, W., Neuman, J. a., Tang, Y. S., Sutton, M. a., Erisman, J. W. and Coheur, P. F.: Towards validation of
824 ammonia (NH₃) measurements from the IASI satellite, *Atmos. Meas. Tech.*, 8(3), 1575–1591, doi:10.5194/amt-
825 8-1575-2015, 2015a.

826
827 Van Damme, M., J. W. Erisman, L. Clarisse, E. Dammers, S. Whitburn, C. Clerbaux, A. J. Dolman, and P.-F.
828 Coheur (2015b), Worldwide spatiotemporal atmospheric ammonia (NH₃) columns variability revealed by
829 satellite, *Geophys. Res. Lett.*, 42, doi:10.1002/2015GL065496.

830
831 Velasco, V., Wood, S. W., Sinnhuber, M., Kramer, I., Jones, N. B., Kasai, Y., Notholt, J., Warneke, T.,
832 Blumenstock, T., Hase, F., Murcray, F. J., and Schrems, O.: Annual variation of strato-mesospheric carbon
833 monoxide measured by ground-based Fourier transform infrared spectrometry, *Atmos. Chem. Phys.*, 7, 1305-
834 1312, doi:10.5194/acp-7-1305-2007, 2007.

835
836 Vigouroux, C., Hendrick, F., Stavrakou, T., Dils, B., De Smedt, I., Hermans, C., Merlaud, A., Scolas, F., Senten,
837 C., Vanhaelewyn, G., Fally, S., Carleer, M., Metzger, J.-M., Müller, J.-F., Van Roozendael, M., and De
838 Mazière, M.: Ground-based FTIR and MAX-DOAS observations of formaldehyde at Réunion Island and
839 comparisons with satellite and model data, *Atmos. Chem. Phys.*, 9, 9523-9544, doi:10.5194/acp-9-9523-2009,
840 2009.

841

842 Wagner, T., Beirle, S., Grzegorski, M. and Platt, U.: Global trends (1996-2003) of total column precipitable
843 water observed by Global Ozone Monitoring Experiment (GOME) on ERS-2 and their relation to near-surface
844 temperature, *J. Geophys. Res. Atmos.*, 111(12), 1–15, doi:10.1029/2005JD006523, 2006.
845

846 Whitburn, S., Van Damme, M., Kaiser, J. W., van der Werf, G. R., Turquety, S., Hurtmans, D., Clarisse, L.,
847 Clerbaux, C. and Coheur, P.-F.: Ammonia emissions in tropical biomass burning regions: Comparison between
848 satellite-derived emissions and bottom-up fire inventories, *Atmos. Environ.*, 1–13,
849 doi:10.1016/j.atmosenv.2015.03.015, 2015.
850

851 Whitburn, S. Van Damme, M., Clarisse, L., Heald, C., Bauduin, S., Hadji-Lazaro, J., Hurtmans, D., Clerbaux,
852 C. and Coheur P.-F.: A flexible and robust IASI-NH 3 retrieval algorithm, 2015 (in preparation)
853

854 Wiacek, A., Taylor, J. R., Strong, K., Saari, R., Kerzenmacher, T. E., Jones, N. B. and Griffith, D. W. T.:
855 Ground-Based Solar Absorption FTIR Spectroscopy: Characterization of Retrievals and First Results from a
856 Novel Optical Design Instrument at a New NDACC Complementary Station, *J. Atmos. Ocean. Technol.*, 24(3),
857 432–448, doi:10.1175/JTECH1962.1, 2007.
858

859 Wood, S. W.: Validation of version 5.20 ILAS HNO₃, CH₄, N₂O, O₃, and NO₂ using ground-based
860 measurements at Arrival Heights and Kiruna, *J. Geophys. Res.*, 107(D24), 8208, doi:10.1029/2001JD000581,
861 2002.
862

863 Zhu, L., Henze, D. K., Cady-Pereira, K. E., Shephard, M. W., Luo, M., Pinder, R. W., Bash, J. O. and Jeong, G.
864 R.: Constraining U.S. ammonia emissions using TES remote sensing observations and the GEOS-Chem adjoint
865 model, *J. Geophys. Res. Atmos.*, 118(8), 3355–3368, doi:10.1002/jgrd.50166, 2013.
866

Tables

Table 1 FTIR stations used in the analysis. The location, longitude, latitude and altitude are given for each station as well as the instrument used for the measurements. Typical emission sources are mentioned in the station specifics tab. The topography describes the geography of the region surrounding the site. N gives the number of observations made during the period of interest. Time period gives the period from which data is used. The last columns describes the used algorithm for the retrieval.

Station Location	Lon	Lat	Altitude (m.a.s.l.)	Instrument	Station specifics	Topography	Time period	N	Retrieval type
Bremen, Germany	8.85E	53.10N	27	Bruker 125 HR	City, fertilizers, livestock	Flat	2008-2015	278	Normal
Toronto, Canada	79.60W	43.66N	174	ABB Bomem DA8	City, fertilizers, biomass burning	On the edge of lake Ontario	2008-2015	1167	Normal
Boulder, United States	105.26W	39.99N	1634	Bruker 120 HR	Fertilizers, biomass burning, livestock	Mountain range to the west	2010-2015	440	Normal
Tsukuba, Japan	140.13E	36.05N	31	Bruker 125 HR	Fertilizers, city	Mostly flat, hills to the north	2014-2015	66	Normal
Pasadena, United States	118.17W	34.20N	460	MKIV_JPL	City, fertilizers, biomass burning	Mountain range to the east	2010-2015	695	Normal
Mexico City, Mexico	99.18W	19.33N	2260	Bruker Vertex 80	City, fires, fertilizers	In between mountain ranges	2012-2015	3980	Normal
St.-Denis, Reunion	55.5E	20.90S	85	Bruker 120 M	Fertilizers, biomass burning, remote	Volcanic	2008-2012	948	Wide
Wollongong, Australia	150.88E	34.41S	30	Bruker 125 HR	Fertilizers, biomass burning, low emissions	Coastal, hills to the west	2008-2015	3641	Wide
Lauder, New Zealand	169.68E	45.04S	370	Bruker 120 HR	Fertilizers, livestock	Hills	2008-2015	1784	Normal

Table 2 Applied data filters to the IASI-NH₃ product.

Filter	Filter Criteria
Elevation	$ \text{FTIRstation} - \text{IASI_Observation} < 300 \text{ m}$
Thermal Contrast	Thermal contrast $> 12 \text{ K}$
Surface Temperature	$T > 275.15 \text{ K}$
IASI-NH ₃ retrieval Error	None
Cloud cover fraction	$< 10\%$
Spatial sampling difference	$50 \text{ km} \rightarrow 10 \text{ km}, \Delta x = 5 \text{ km}$
Temporal sampling difference	$< 90 \text{ minutes}$

Table 3. Summarized results of the comparison between FTIR-NH₃ and IASI-NH₃ total columns within the coincidence criteria threshold (xdiff < 25 km, tdiff < 90minutes). N is the number of averaged total columns, **MRD** is the Mean Relative Difference (in %), **r** and **slope** are the correlation coefficient and slope of the linear regression.

Sites	N	MRD in % (rms 1 σ)	r	slope
Bremen	53	-22.5 \pm (54.0)	0.83	0.60
Toronto	170	-46.0 \pm (47.0)	0.79	0.84
Boulder	38	-38.2 \pm (43.5)	0.76	1.11
Tsukuba	15	-28.3 \pm (35.6)	0.67	0.57
Pasadena	16	-47.9 \pm (30.1)	0.59	0.83
Mexico	65	-30.8 \pm (43.9)	0.64	1.14
St.-Denis	20	-61.3 \pm (78.7)	0.65	1.26
Wollongong	62	6.0 \pm (74.3)	0.47	0.92
Lauder	108	-29.7 \pm (57.3)	0.55	0.77
Combined	547	-32.4\pm(56.3)	0.80	0.73

Figures

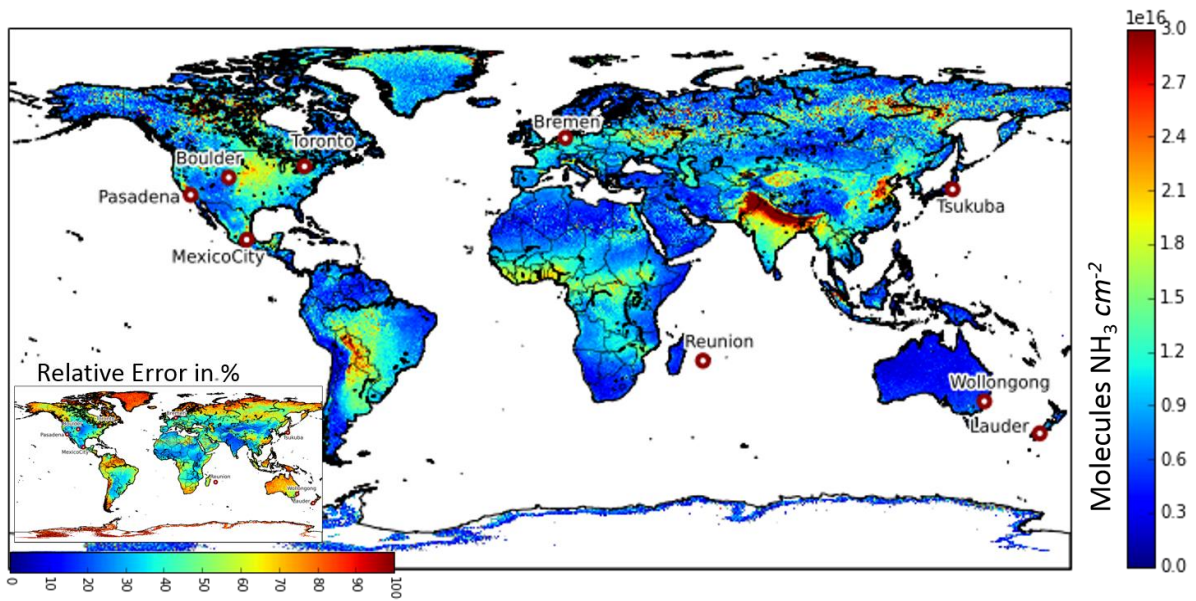


Figure 1. Mean IASI-NH₃ total column distribution for the period between January 2008 and January 2015. The total columns are a weighted average of the individual observations weighted with the relative error. Red circles indicate the positions of the FTIR stations.

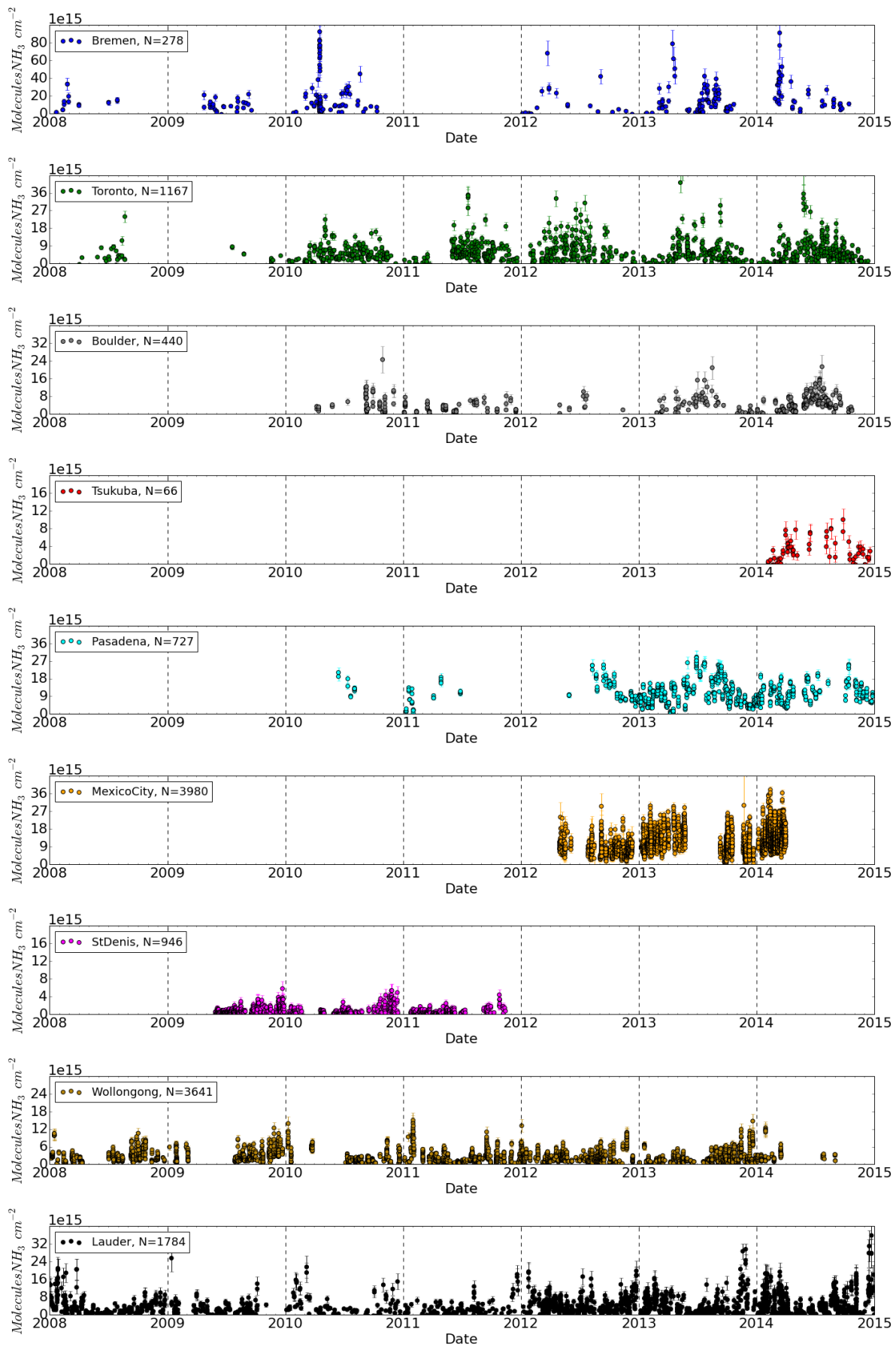


Figure 2. FTIR retrieved NH₃ Total Columns (in *molecules cm⁻²*). Note, the labels on the vertical axis vary for each site.

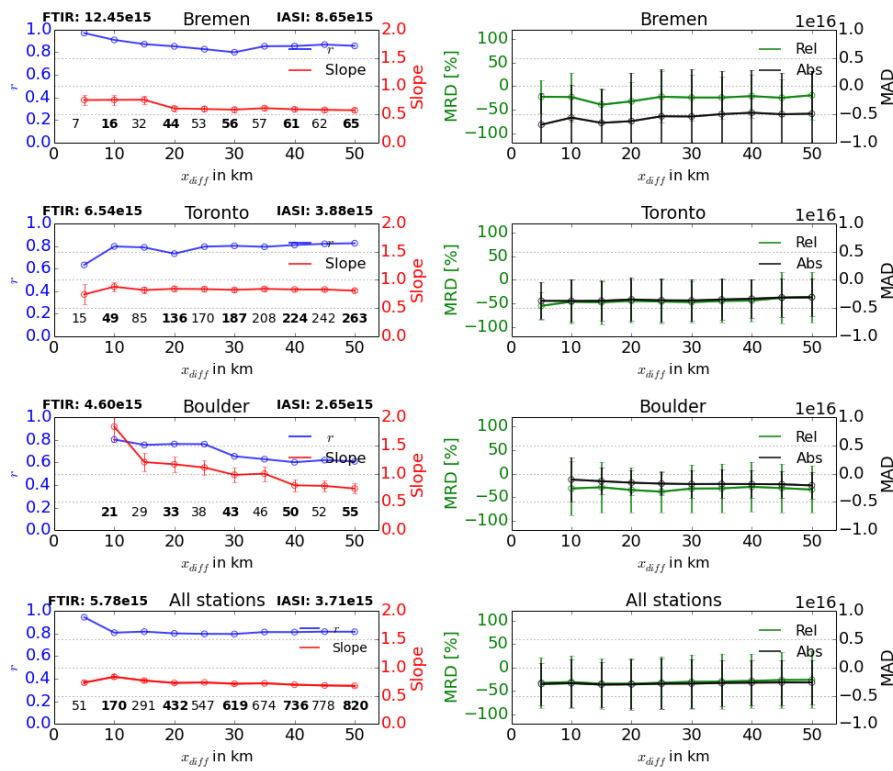


Figure 3. Correlation r (Blue lines, left figures), slope (Red lines, left figures) regression results, Mean Relative Difference (MRD, green lines, right figures) and Mean Absolute Difference (MAD, black lines, right figures) between IASI and FTIR observations as a function of x_{diff} for a selection of sites. Bars indicate the standard deviation of the slope of the individual regression results. The numbers in the bottom of each subfigure show the number of matching observations. The numbers on the left and right side of the stations name give the mean FTIR and IASI total columns for a $x_{diff} < 25$ km.

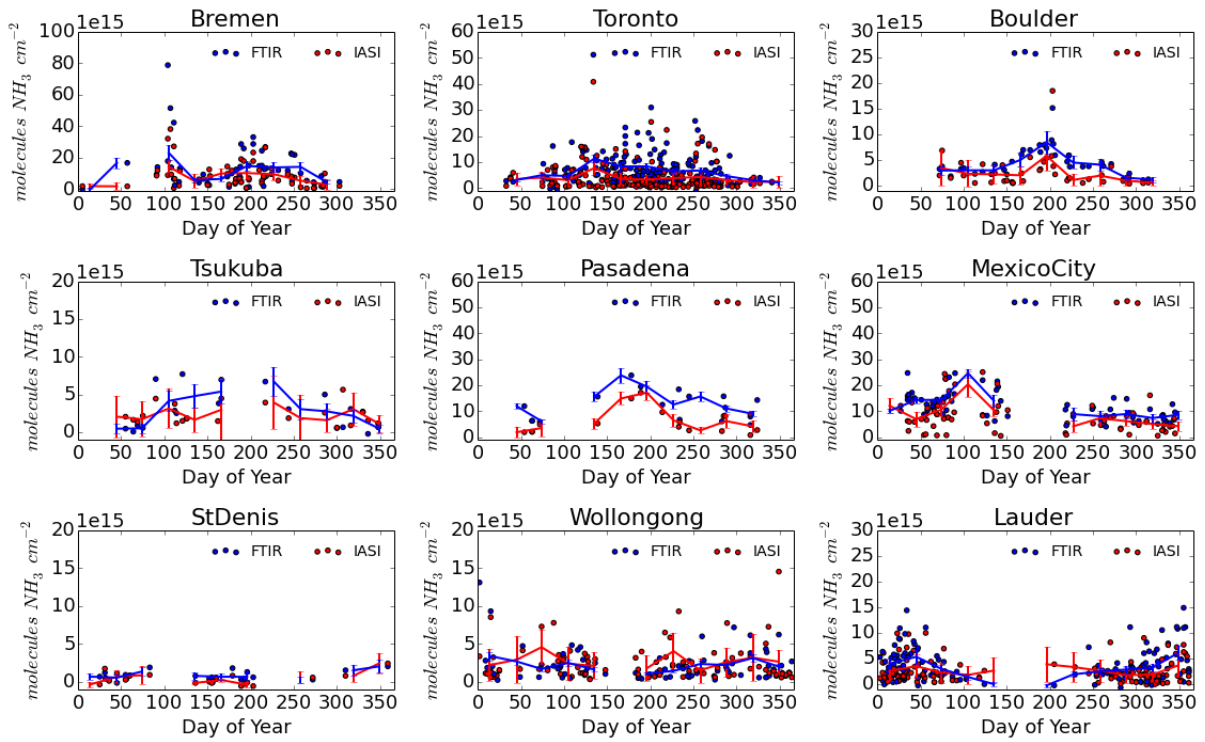


Figure 4. Time series of NH_3 for IASI and FTIR datasets with $\text{xdiff} < 25$ km and $\text{tdiff} < 90$ minutes (FTIR: Blue and IASI: Red). Scattered values are the observations for each day of year (multiple years of observations). The lines show the monthly mean total columns of the respective sets.

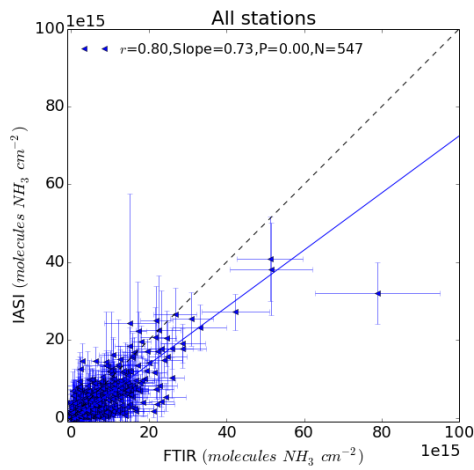


Figure 5. Correlations between the FTIR and IASI total columns with filters thermal contrast $> 12\text{K}$, $\text{tdiff} < 90$ min, $\text{xdiff} < 25$ km. The trend line shows the results of the regression analysis.

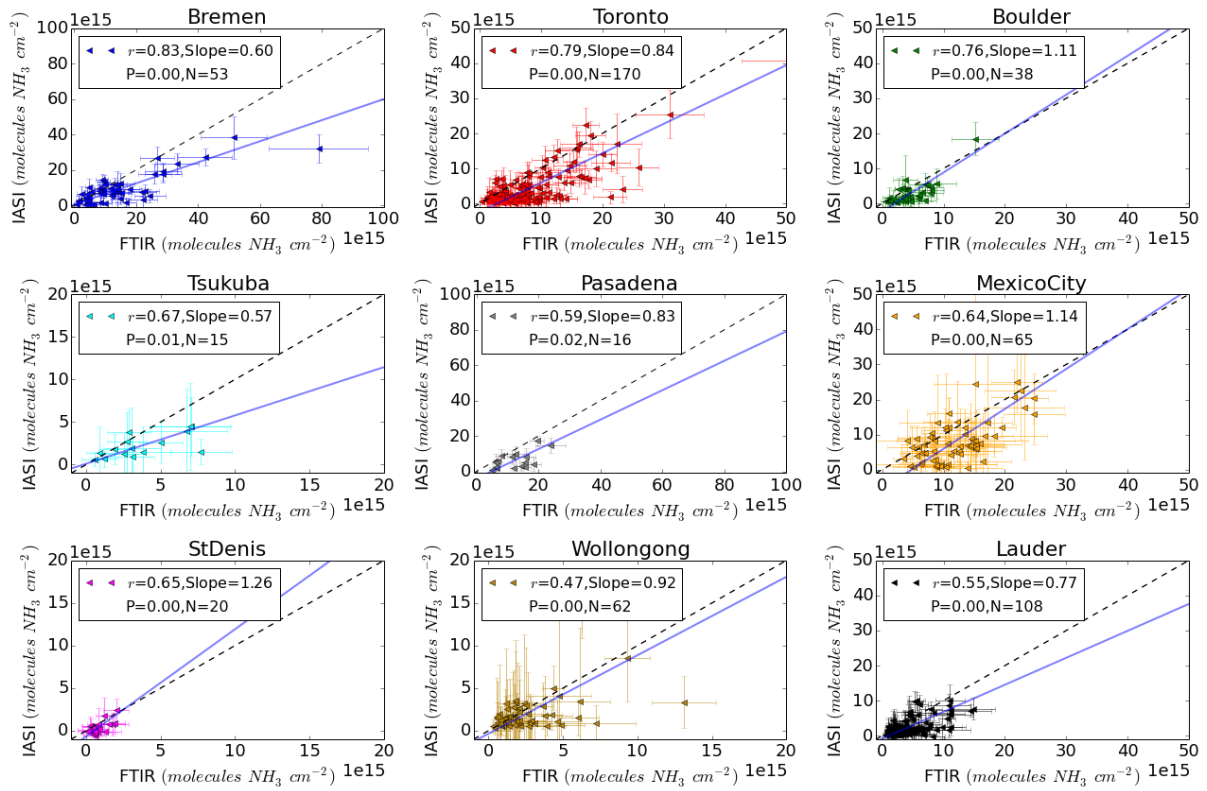


Figure 6. Correlations between the FTIR and IASI total columns with filters thermal contrast > 12 , $tdiff < 90min$, $xdiff < 25 km$. The trend lines show the results of the regression analysis.

Appendix A

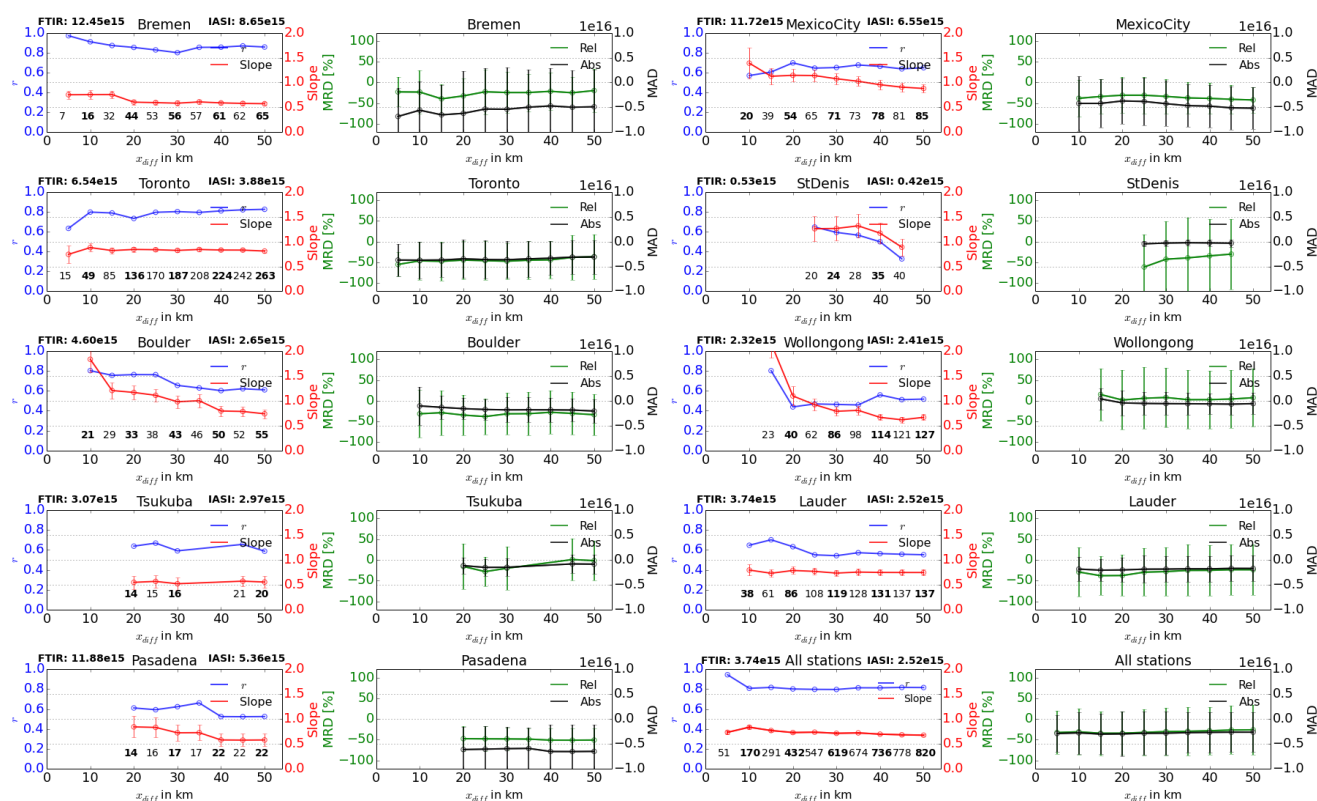


Figure A1. Correlation r (Blue lines, left figures), slope (Red lines, left figures) regression results, Mean Relative Difference (MRD, green lines, right figures) and Mean Absolute Difference (MAD, black lines, right figures) between IASI and FTIR observations as a function of x_{diff} for all sites. Bars indicate the standard deviation of the slope of the individual regression results. The numbers in the bottom of each subfigure show the number of matching observations. The numbers on the left and right side of the stations name give the mean FTIR and IASI total columns for a $x_{diff} < 25$ km.

This section further covers the other stations, in addition to the sites covered by section 3.1.

The results for Mexico City show an overall constant correlation coefficient except for small criteria < 20 km. The slope also decreases towards values seen at other stations. This effect could be due to a large number of sources inside the city, i.e. automobile and agricultural emissions in and near the city, increasing the heterogeneity of the found column totals. Reunion and Tsukuba have few coincident observations leading to only a few significant comparisons. This, combined with the low concentrations measured at Reunion leads to large differences in the mean and standard deviations of the subsequent x_{diff} sets. The Reunion and Wollongong observations are at the sensitivity limit of the IASI-NH₃ retrieval which limits the usefulness of the sites for the validation. As there are only a few observations for Tsukuba it is hard to make meaningful conclusions for the variability around the site.